

## The X/Ka-band Extragalactic Reference Frame

C. García-Miró<sup>1</sup>, J.E. Clark<sup>2</sup>, S. Horiuchi<sup>3</sup>, C.S. Jacobs<sup>2</sup>, A. Romero-Wolf<sup>2</sup>,  
L.G. Snedeker<sup>4</sup>, I. Sotuela<sup>1</sup>

<sup>1)</sup> *Madrid Deep Space Communications Complex/NASA, INTA, Madrid, Spain*

<sup>2)</sup> *Jet Propulsion Laboratory/NASA, California Institute of Technology, Pasadena, CA*

<sup>3)</sup> *Canberra Deep Space Communications Complex/NASA, C.S.I.R.O., Canberra, Australia*

<sup>4)</sup> *Goldstone Deep Space Communications Complex/NASA, ITT Exelis, Monrovia, CA*

Contact author: C. García-Miró, e-mail: [cgmiro@mdscc.nasa.gov](mailto:cgmiro@mdscc.nasa.gov)

### Abstract

We have constructed an X/Ka-band (8.4/32 GHz) celestial reference frame using fifty-nine  $\sim$ 24-hour sessions with the Deep Space Network. We detected 469 sources covering the full 24 hours of right ascension and declinations down to  $-45^\circ$ . Comparison of 450 X/Ka sources in common with the S/X-band (2.3/8.4 GHz) ICRF2 shows weighted RMS (wRMS) agreement of 194 micro-arcsec ( $\mu$ as) in  $\alpha \cos \delta$  and 270  $\mu$ as in  $\delta$ . There is evidence for systematic errors at the 100  $\mu$ as level. Known errors include limited SNR, lack of phase calibration, troposphere mismodeling, and limited southern geometry. Compared to X-band, Ka-band allows access to more compact source morphology and reduced core shift. Existing X/Ka data and simulated Gaia data predict a frame tie precision of 10-15  $\mu$ as (1- $\sigma$ , per 3-D rotation component) with anticipated improvements reducing that to 5-10  $\mu$ as per component.

### 1. Introduction

Celestial reference frames help us to navigate in deep space just as the Global Positioning System (GPS) helps us to navigate here on Earth. The analogy is not only casual; the importance of the latter in our normal day life is analogous to the importance of the former for astrophysical studies and spacecraft navigation. Celestial reference frames are needed to define the coordinates of every celestial object, to reference astronomical events such as eclipses or occultations, and to navigate space probes around the Solar System or to calculate spacecraft instrument fields of view as they point, for instance, towards a planet. Even GPS satellites themselves need to have their orbits defined with respect to a quasi-inertial reference frame.

Motivated by the need to navigate inter-planetary space probes, the NASA Deep Space Network (DSN) constructs VLBI radio reference frames to measure spacecraft positions and motions. An earlier version of the DSN catalog was built at S/X-bands and is still periodically maintained. Because higher data rate requirements for spacecraft telemetry are driving the DSN to higher frequencies from X to Ka-band (32 GHz), the radio catalog presented here was realized at X/Ka bands. Fortunately, the jump to Ka-band has astrophysical advantages which should eventually allow more accurate position determinations. We also note that international Ka-band acceptance is growing. About 20 antennas around the world have, will have, or are considering acquiring 32 GHz capability. Jacobs *et al.* (these proceedings) discuss the potential for a worldwide Ka-band VLBI network capable of high resolution imaging and astrometry of the most compact regions in Active Galactic Nuclei.

This paper is organized as follows. Section 2 presents the advantages and disadvantages of Ka-band observations. Section 3 describes the Ka-band VLBI observations and compares our VLBI Ka-band frame with current radio-based celestial frames. Section 4 discusses the potential for improving the geometry of our network by adding a southern station. Section 5 presents the potential for a frame tie to the Gaia optical reference frame.

## 2. Reference Frame Realization at Higher Radio Frequencies

The recent move of radio observations towards higher frequencies is beginning to provide very promising astrometric results (Lanyi *et al.*, 2010, Charlot *et al.*, 2010). Ka-band, approximately a factor of four higher than the usual X-band, has several remarkable advantages. For our work in the DSN, the driver is the increase of telemetry data rates and the usage of smaller and lighter radio frequency systems in the spacecraft. The spatial distribution of the observed source’s flux density becomes significantly more compact (Charlot *et al.*, 2010) and should therefore lead to more stable positions. S-band Radio Frequency Interference (RFI) problems are avoided. In addition, the ionosphere and solar plasma effects on group delay and signal coherence are reduced by a factor of  $\sim 15$  allowing observations closer to the Sun and the Galactic Center.

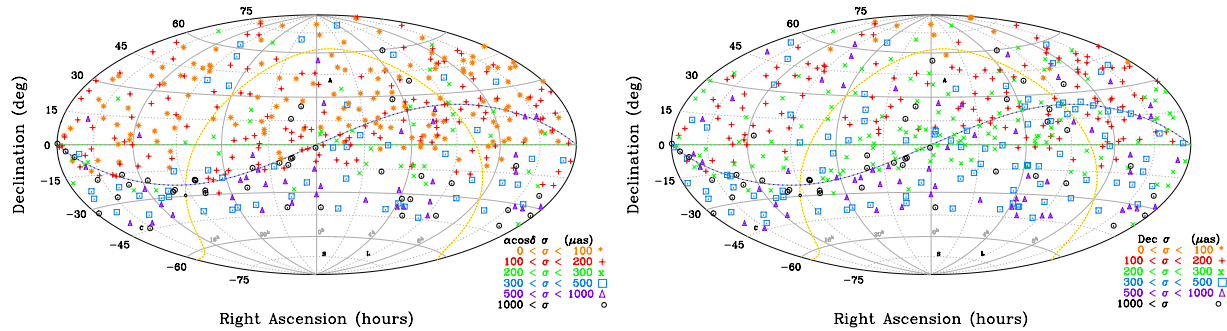
The increase in frequency also implies several disadvantages. It moves the observer closer to the water vapor line at 22 GHz and thus increases the system temperature to up to 10–15 K per atmosphere or more, thereby greatly increasing sensitivity to poor weather. Furthermore, the sources themselves are in general weaker, and many sources are resolved. Also, the coherence times are shortened so that practical integration times are a few minutes or less, and lastly the antenna pointing accuracy requirements must be tightened by the same factor of four. The combined effect of these disadvantages lowers the system sensitivity. Fortunately, advances in recent years in recording technology (e.g., Whitney *et al.*, these proceedings) make it feasible and affordable to offset these losses in sensitivity by recording at higher data rates.

## 3. X/Ka VLBI Observations and Accuracy

The results presented here are from fifty-nine Very Long Baseline Interferometry (VLBI) observing sessions of  $\sim 24$  hour duration done from July 2005 until February 2012 using NASA’s Deep Space Stations (DSS) 25 or 26 in Goldstone, California to either DSS 34 in Tidbinbilla, Australia or DSS 55 or DSS 54 outside Madrid, Spain to form interferometric baselines of 10,500 and 8,400 km length, respectively. We have detected 469 extragalactic radio sources which covered the full 24 hours of  $\alpha$  and  $\delta$  down to  $-45^\circ$ . These sources are plotted using a Hammer-Aitoff projection to show their locations in the sky (Figure 1). Note that both  $\alpha$  (Figure 1a) and  $\delta$  (Figure 1b) precisions get worse as one moves southward. This is a result of having significantly less data on the California to Australia baseline combined with the need to observe sources closer to the horizon as declination moves south thus incurring greater error from higher system temperatures and tropospheric mismodeling. Jacobs *et al.* (2011) give details on the VLBI observation configuration, data reduction, and delay modeling.

An independent estimate of the position errors was obtained by comparing our X/Ka-band positions to the S/X-based ICRF2 (Ma *et al.*, 2009). For 450 common sources, the weighted RMS (wRMS) differences are  $\sim 194 \mu\text{as}$  in  $\alpha \cos \delta$  and  $\sim 270 \mu\text{as}$  in  $\delta$ . Apart from the limited southern coverage, the major contributions to the errors in our measurements are the limited SNR and

poorly calibrated instrumentation and troposphere effects. We plan to reduce these last three errors by improving the recording rates, installing Ka-band phase calibrators and making use of an advanced water vapor radiometer, respectively. The following section discusses the southern geometry issue.



a) Right Ascen. formal uncertainty:  $\sigma_{\alpha \cos \delta}$ .

b) Declination formal uncertainty:  $\sigma_{\delta}$ .

Figure 1. Distribution of 469 X/Ka sources plotted using a Hammer-Aitoff projection to show their locations in the sky.  $\alpha = 0$  is at the center. The ecliptic plane is shown by the dashed blue-gray line, and the Galactic plane is indicated by the yellow-red dashed line. The sources are color and symbol coded according to their  $1\text{-}\sigma$  formal  $\alpha \cos \delta$  and  $\delta$  uncertainties with the value ranges indicated in the legend. Note the drop in precision below  $\delta = -20^\circ$  where the California–Spain baseline coverage can no longer reach.

#### 4. Towards X/Ka-band Southern Geometry Improvement

The DSN is an excellent instrument for astrometric measurements due to its high sensitivity (large apertures, low system temperatures, and high data rates) and long baselines ( $> 8000$  km). However, the DSN's single southern site limits the southernmost observed declinations ( $> -45^\circ$ ). In order to better understand the impact of southern geometry, we have simulated the effect of adding a second southern station (Bourda *et al.*, 2010). Data from 50 real X/Ka sessions were augmented by simulated data for 1000 group delays each with SNRs = 50 on a  $\sim 9000$  km baseline: Australia to South America or South Africa (Figure 2). The resulting solution extended the  $\delta$  coverage to the south polar cap region:  $-45$  to  $-90^\circ$ . Precision in the south cap region was  $\sim 200 \mu\text{as}$  (1 nrad), and in the mid-south precision was 200–1000  $\mu\text{as}$ , all with just a few days of observing. We conclude that adding a second southern station would greatly aid our X/Ka frame's coverage and accuracy. In fact, the resulting four station network should compete well in astrometric accuracy with the historical S/X network and its ICRF2. Accordingly, efforts are now under way to improve the DSN southern coverage, and we have initiated a project to survey candidate sources at Ka-band in the Southern Hemisphere (Horiuchi *et al.*, these proceedings).

#### 5. Gaia Frame Tie Simulations

The future Gaia optical reference frame (Lindgren *et al.*, 2008) will also use quasars as defining sources, most of them optically bright. We present here a simulated frame tie between a set of common sources in our X/Ka frame and the Gaia frame. The Gaia mission will survey a billion

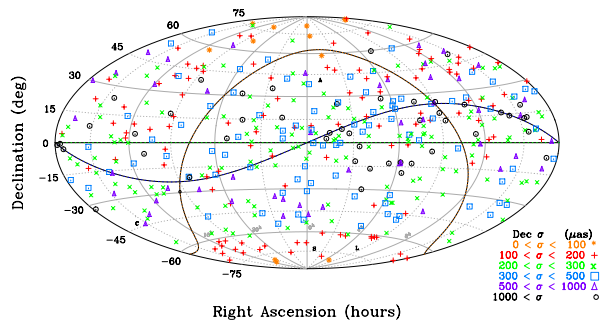


Figure 2. Simulated data for 1000 delays added to 50 real sessions completes southern coverage in the south polar cap  $-45^\circ < \delta < -90^\circ$ . Note that south circumpolar sources ( $\delta < -60^\circ$ ) achieve  $200 \mu\text{as}$  precision within a few days.

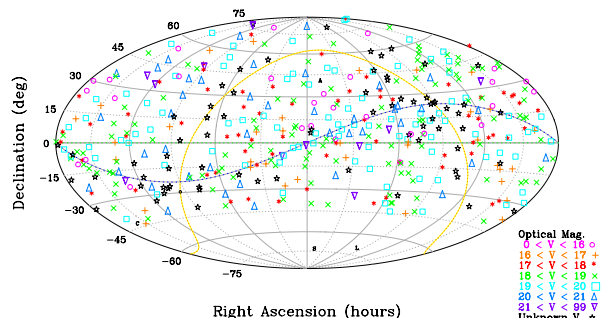


Figure 3. Visual magnitude of optical counterparts for distribution of 469 X/Ka sources. The  $V$  magnitude scale is defined in the legend. Note the large number of sources lacking optical identifications near the galactic plane, especially near its center and anti-center.

objects down to  $V = 20$  visual magnitude (500–600 nm), with accuracies ranging from  $25 \mu\text{as}$  at  $V = 16$  to  $\sim 200 \mu\text{as}$  at  $V = 20$ . The sample will include about 500,000 quasars of which  $\sim 2000$  are expected to be both optically bright ( $V < 18$ ) and radio loud (30–300+ mJy).

A potential tie between the optical Gaia and the radio reference frames requires a deep understanding of the different emitting regions in relativistic jets. For an ensemble of relativistic electrons with an energy power-law distribution and subjected to synchrotron radiative losses that decrease their lifetimes with increasing energy, the observed flux density distribution becomes more compact but weaker at higher observing frequencies (Konigl, 1981). Moreover, opacity effects, which alter the position of the core, are greatly reduced for higher frequencies. The expected core shift for phase delays from X to Ka is  $\sim 100 \mu\text{as}$  and from Ka to optical is  $\sim 25 \mu\text{as}$ . However, Porcas (2009) argues that, under minimum energy conditions or (near) equi-partition of particle and magnetic energy in the jets (Pacholczyk, 1970), the effect in group delay is several times smaller than in phase delay. Thus our X/Ka group delay results are expected to have little core-shift.

Table 1. Optical magnitude categories of DSN X/Ka sources.

Description	Magnitude range	Number	Percent
Bright	$0 < V < 18$	132	29%
Detectable	$18 < V < 20$	213	45%
Undetectable	$V > 20$	53	11%
Unmeasured	$V$ unknown	71	15%

Based on Veron-Cetty & Veron (2010), our X/Ka catalog has 345 sources with optical counterparts bright enough to be detected by Gaia ( $V < 20$  mag, Table 1, Figure 3). Of these, 132 are bright by Gaia standards ( $V < 18$ ). Using existing X/Ka-band position uncertainties and simulated Gaia uncertainties (Gaia (2012) *corrected for ecliptic latitude, but not for V–I color*), we did a covariance study which predicts that the 3-D rotation between the X/Ka frame and the Gaia frame could be estimated with a precision of 10–15  $\mu\text{as}$  per rotation angle ( $1-\sigma$ ). The result is

dominated by X/Ka uncertainties which have potential for a factor of two or more improvement by the time of the final Gaia catalog in 2021. Thus a frame tie precision of 5–10  $\mu\text{as}$  may be possible.

## 6. Conclusions

We have detected 469 sources at X/Ka-band (8.4/32 GHz). For the 450 sources common to X/Ka and the S/X-based ICRF2, we find positional agreement of 194  $\mu\text{as}$  (0.9 nrad) in  $\alpha \cos \delta$  and 270  $\mu\text{as}$  (1.3 nrad) in  $\delta$  with zonal errors of  $\sim 100 \mu\text{as}$  (0.5 nrad). Improvements in data rates and instrumental calibration are projected to allow better than 200  $\mu\text{as}$  (1 nrad) accuracy within the next few years. Simulations of adding another southern station predict better than 200  $\mu\text{as}$  accuracy for the southern polar cap within a very short time of collecting data from an all southern baseline. This gives hope that better than 100  $\mu\text{as}$  accuracy over the full sky might be achieved within a few years of adding a southern baseline, yielding results comparable to Gaia for objects common to both techniques and thus optimizing a tie between the two frames.

## Acknowledgements

Research done in part under NASA contract. Sponsorship by U.S. Government, and our respective institutes acknowledged. Copyright ©2012. All Rights Reserved.

## References

- [1] Bourda, G., et al., ‘Future Radio Reference Frames & Gaia Link,’ Proc. ELSA Conf., France, 2010.
- [2] Charlot, P., et al., ‘CRF at 24 & 43 GHz II. Imaging,’ AJ, 139, 5, 1713, 2010.
- [3] Gaia, <http://www.rssd.esa.int/index.php?project=GAIA&page=Science.Performance>, 2012.
- [4] Horiuchi, S., et al., ‘32 GHz CRF Survey Dec  $< -45^\circ$ ,’ Proc. of IVS GM, Madrid Spain, 2012.
- [5] Jacobs, C.S., et al., ‘XKa CRF,’ Proc. 20<sup>th</sup> EVGA, Alef, Bernhart, Nothnagel (eds.), 166, 2011.
- [6] Jacobs, C.S., et al., ‘Ka-band Worldwide VLBI Network,’ Proc. of IVS GM, Madrid, Spain, 2012.
- [7] Konigl, A., ‘Relativistic Jets as X-ray and gamma-ray Sources,’ ApJ, 243, 700, 1981.
- [8] Lanyi, et al., ‘CRF at 24 & 43 GHz I. Astrometry,’ AJ, 139, 5, 1695, 2010.
- [9] Lindegren, et al., ‘Gaia Mission: Science, Organiz., Status,’ IAU 248, Wenjin et al. (eds.), 217, 2008.
- [10] Lindegren, et al., ‘The astrometric core solution for the Gaia mission,’ A&A, 538, Feb. 2012.
- [11] Ma, C., et al., ‘2<sup>nd</sup> Realization of ICRF by VLBI,’ IERS Tech Note 35, Frankfurt, Germany, 2009.
- [12] Pacholczyk, A.G., *Radio Astrophysics*, W.H. Freeman, 1970.
- [13] Porcas, R.W., ‘Radio Astrometry with Chromatic AGN Core Positions,’ A&A, 505, L1-L4, 2009.
- [14] Veron-Cetty & Veron, ‘Catalogue of quasars and active nuclei: 13<sup>th</sup> edition,’ A&A, 51, Feb. 2010.
- [15] Whitney, A., et al, ‘Mark 6 Next Gen VLBI Data System,’ Proc. of IVS GM, Madrid, Spain, 2012.